ACS Medicinal Chemistry Letters

pubs.acs.org/acsmedchemlett Letter

Characterization and Optimization of Benzimidazopyrimidine and Pyridoimidazopyridine Derivatives as Tau-SPECT Probes

Hiroyuki Watanabe,* Takeaki Kishimoto, Sho Kaide, Yuta Tarumizu, Haruka Tatsumi, Shimpei Iikuni, and Masahiro Ono*

Cite This: ACS Med. Chem. Lett. 2021, 12, 805−811 Read Online

ACCESS | Metrics & More | Article Recommendations | Supporting Information

ABSTRACT: The accumulation of hyperphosphorylated tau protein in the brain is regarded as one of the hallmarks of Alzheimer's disease (AD). In vivo imaging of tau aggregates is helpful for diagnosis and monitoring of the progression of AD. In this study, we designed and synthesized novel radioiodinated benzimidazopyrimidine (BIPM) and pyridoimidazopyridine (PIP) derivatives with a monomethylamino, monoethylamino, monopropylamino, or diethylamino group as tau imaging probes for single-photon-emission computed tomography (SPECT). On in vitro autoradiography with AD brain sections, [^{125}I]PIP-NHMe showed the highest selective binding affinity for tau aggregates among the radioiodinated BIPM and PIP derivatives. In a biodistribution study using normal mice, [^{125}I]PIP-NHMe and [^{125}I]PIP-NHEt displayed high initial uptake (6.62 and 6.86% ID/g, respectively, at 2 min postinjection) into and rapid clearance from the brain, with brain$_{2\ min}$/brain$_{30\ min}$ ratios of 38.9 and 28.6, respectively. These results suggest that [^{123}I]PIP-NHMe may be a novel SPECT probe that is useful for detecting tau aggregates in the AD brain.

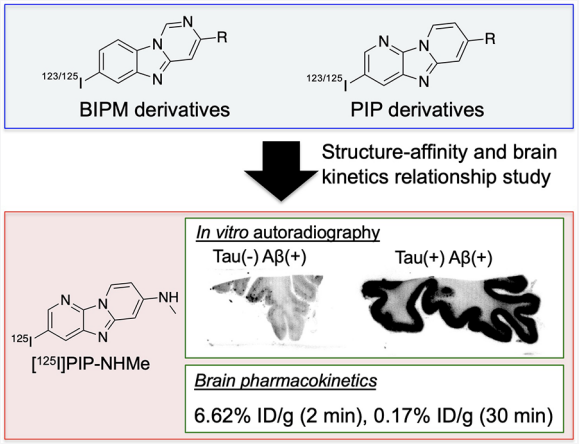

KEYWORDS: *Tau imaging probe, Alzheimer's disease, SPECT, alkylamino group*

Alzheimer's disease (AD) is the most common neurocognitive disorder, and the number of patients worldwide has been projected to increase from 47 million in 2015 to more than 132 million in 2050.[1,2] However, methods for the diagnosis and treatment of AD have not been established. The accumulation of hyperphosphorylated tau protein in the brain is the main feature of AD and tauopathies such as progressive supranuclear palsy, corticobasal degeneration, and pick disease[3] and is closely associated with cognitive impairment. Nuclear medicine techniques, such as positron emission tomography (PET) and single-photon-emission computed tomography (SPECT) can provide pathophysiological information on a living subject noninvasively. Therefore, over the past few years, various PET probes targeting tau aggregates have been developed and evaluated with regard to their utility for diagnosis and monitoring of the progression of AD.[4−7] Among them, [^{18}F]AV-1451 (flortaucipir or T807), which is a first-generation tau-PET probe, and the second-generation tau-PET probes [^{18}F]MK-6240, [^{18}F]RO-948, [^{18}F]PI-2620, [^{18}F]GTP1, and [^{18}F]PM−PBB3 showed potential for imaging of tau aggregates in AD brains.[8−13] Compared with PET, SPECT is more convenient because of the number of facilities and its use of radionuclides with a longer half-life than PET. However, no SPECT probes that target tau aggregates have been tested clinically.

In our exploratory research for the development of novel tau imaging probes, we found that benzimidazopyridine (BIP), which is a fused nitrogen tricyclic scaffold, shows potential as a backbone for useful tau imaging probes for SPECT.[14] Structure−affinity and brain kinetics relationship studies revealed that BIP derivatives with an alkylamino group showed favorable binding affinity for tau aggregates and brain pharmacokinetics in the murine brain.[15,16] Additionally, we recently reported that benzimidazopyrimidine (BIPM) and pyridoimidazopyridine (PIP), which are also categorized as fused nitrogen tricyclic scaffolds, are novel scaffolds for the development of tau imaging probes.[17] The radioiodinated BIPM and PIP derivatives with a dimethylamino group ([^{125}I]BIPM-NMe$_2$ and [^{125}I]PIP-NMe$_2$) displayed selective in vitro binding affinity for tau against β-amyloid (Aβ) aggregates and favorable

Received: January 29, 2021
Accepted: April 20, 2021
Published: April 26, 2021

https://doi.org/10.1021/acsmedchemlett.1c00071
ACS Med. Chem. Lett. 2021, 12, 805−811

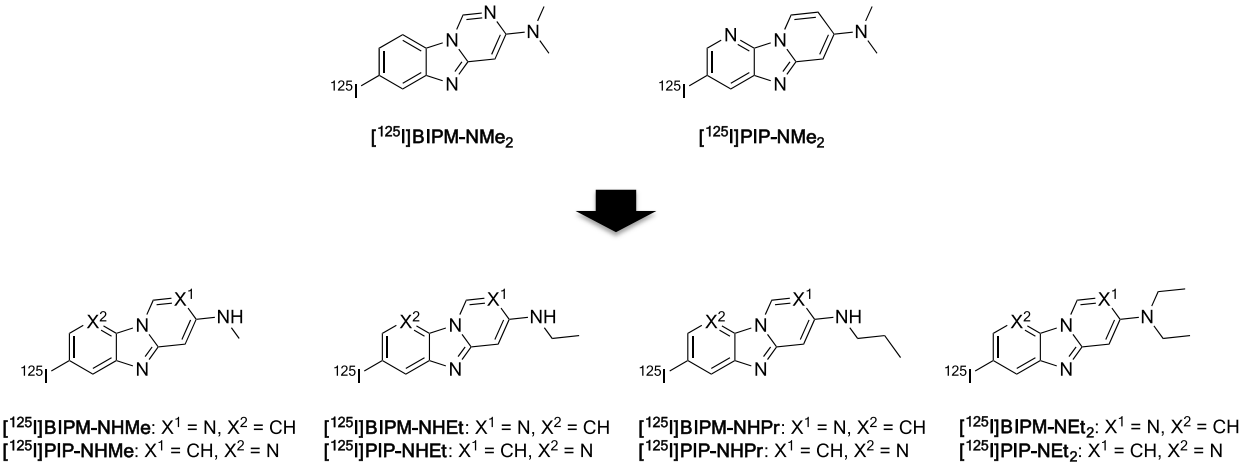

Figure 1. Chemical structures of radioiodinated BIPM and PIP derivatives.

Scheme 1. Synthetic Route to BIPM and PIP Derivatives[a]

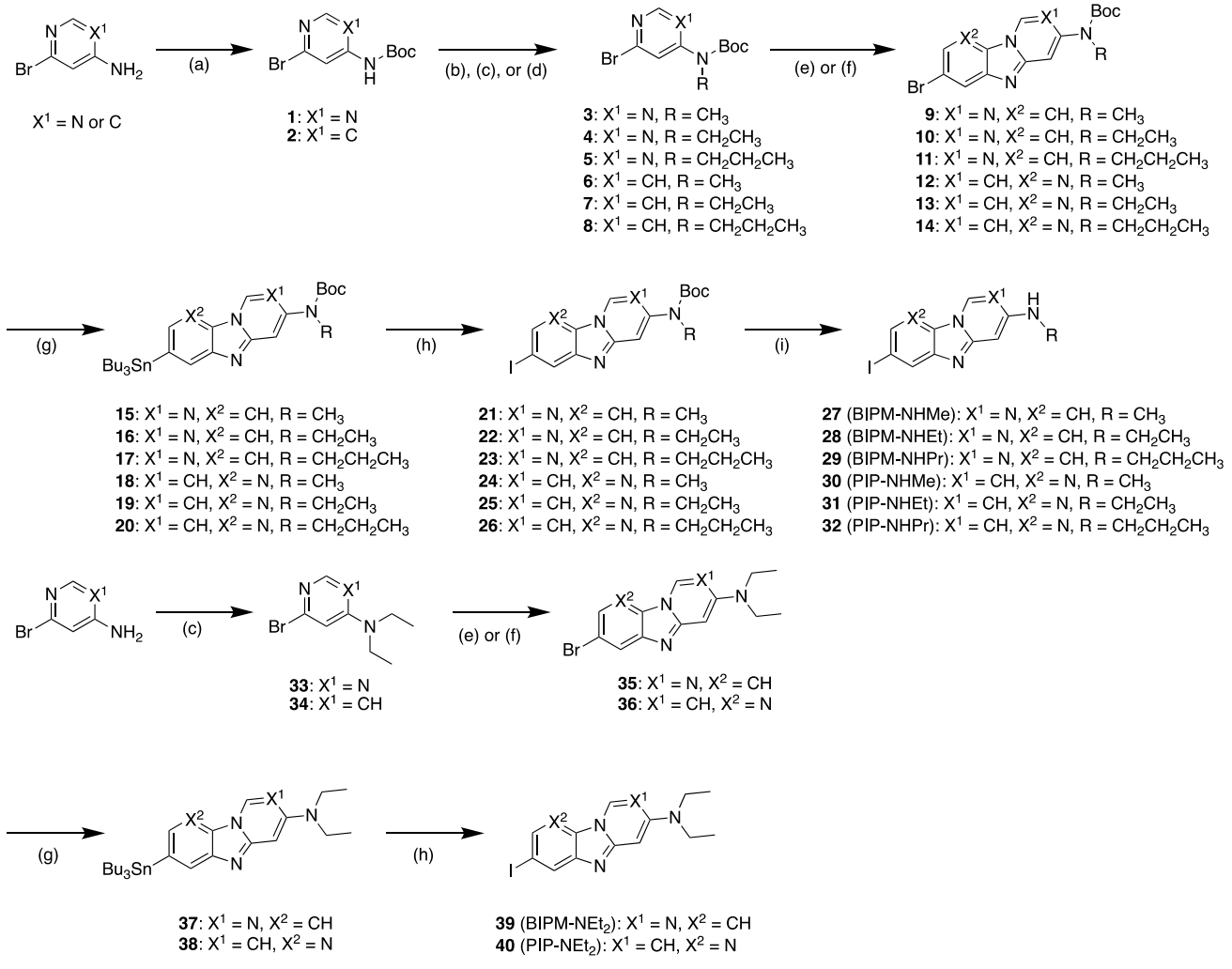

[a]Reagents: (a) di-*tert*-butyl dicarbonate, *N*,*N*-dimethylpyridine-4-amine, Et_3N, THF; (b) CH_3I, NaH, DMF; (c) CH_3CH_2I, NaH, DMF; (d) $CH_3CH_2CH_2I$, NaH, DMF; (e) 2,5-dibromoaniline, CuI, Cs_2CO_3, 1,10-phenanthroline, xylene; (f) 2,5-dibromopyridine-3-amine, CuI, Cs_2CO_3, 1,10-phenanthroline, xylene; (g) bis(tributyltin), $Pd(PPh_3)_4$, dioxane, Et_3N; (h) I_2, $CHCl_3$, (i) TFA, CH_2Cl_2.

pharmacokinetics in the murine brain. However, we have not evaluated BIPM and PIP derivatives with other alkylamino groups. Both the binding affinity for tau aggregates and brain pharmacokinetics of low-molecular-weight compounds such as BIPM and PIP may be influenced by their subtle structural changes. In order to characterize and optimize BIPM and PIP derivatives as SPECT probes that target tau aggregates, we designed and synthesized novel radioiodinated BIPM and PIP

https://doi.org/10.1021/acsmedchemlett.1c00071
ACS Med. Chem. Lett. 2021, 12, 805−811

Scheme 2. Radioiodination Reactions of BIPM and PIP Derivatives[a]

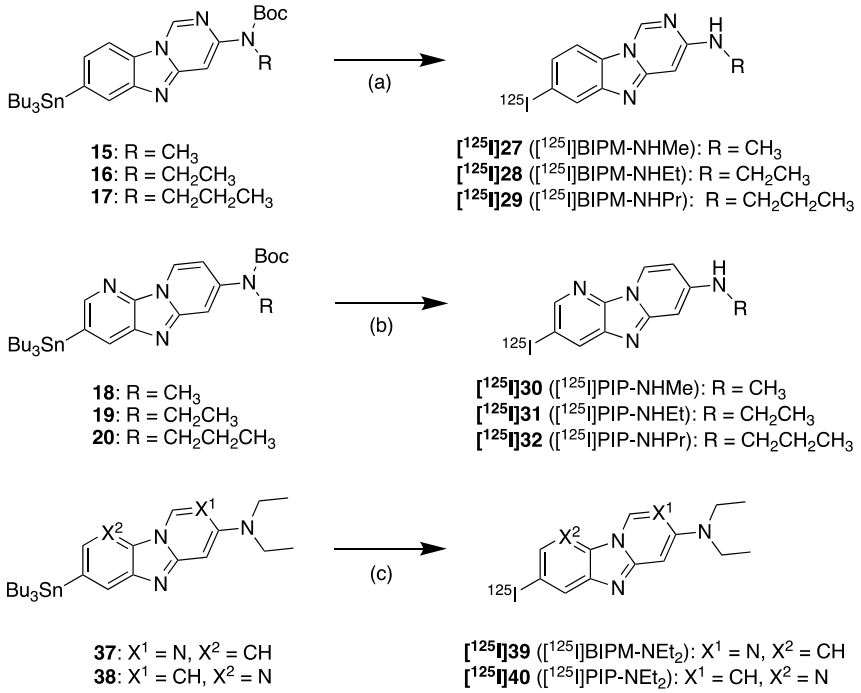

[a]Reagents: (a) (1) [^{125}I]NaI, H_2O_2, 1 N HCl, EtOH; (2) TFA, $CHCl_3$; (b) (1) [^{125}I]NaI, acetic acid, *N*-chlorosuccinimide, MeOH; (2) TFA, $CHCl_3$; (c) [^{125}I]NaI, H_2O_2, 1 N HCl, EtOH.

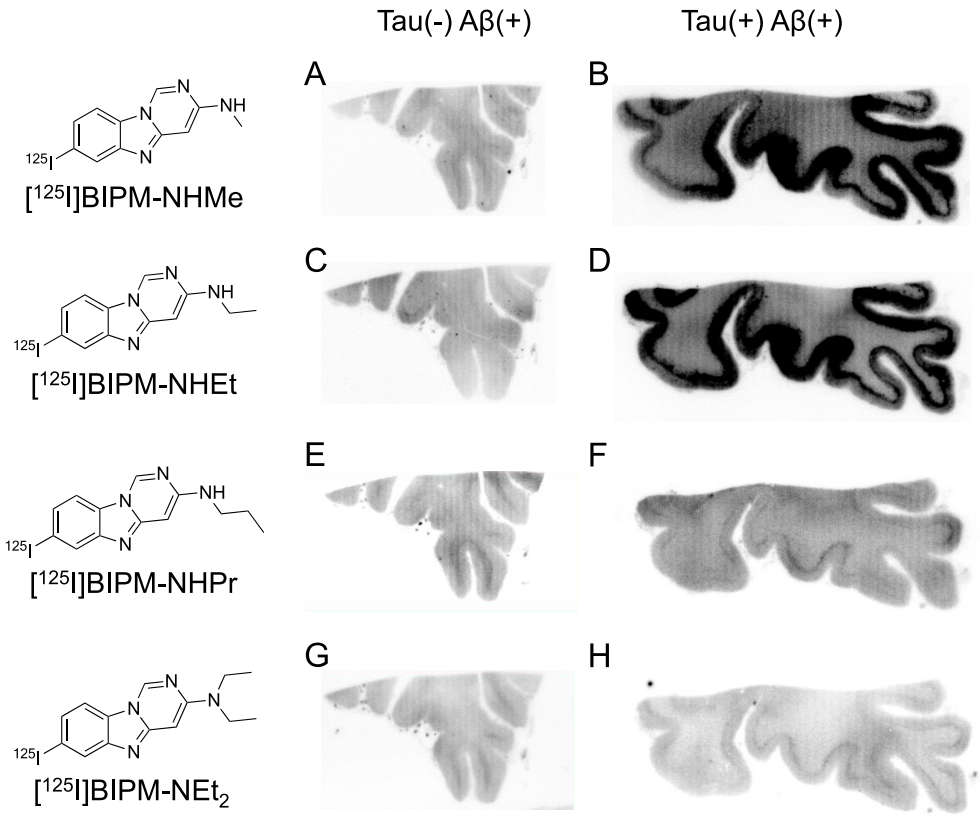

Figure 2. Comparison of in vitro autoradiography of (A, B) [^{125}I]**27** ([^{125}I]BIPM-NHMe), (C, D) [^{125}I]**28** ([^{125}I]BIPM-NHEt), (E, F) [^{125}I]**29** ([^{125}I]BIPM-NHPr), and (G, H) [^{125}I]**39** ([^{125}I]BIPM-NEt_2) in brain sections from an AD patient. A, C, E, and G show results in Aβ(+)/tau(−) brain sections. B, D, F, and H show results in Aβ(+)/tau(+) brain sections.

derivatives with monomethylamino, monoethylamino, monopropylamino, and diethylamino groups (Figure 1) and evaluated their affinity for tau aggregates and in vivo pharmacokinetics in the murine brain.

https://doi.org/10.1021/acsmedchemlett.1c00071
ACS Med. Chem. Lett. 2021, 12, 805−811

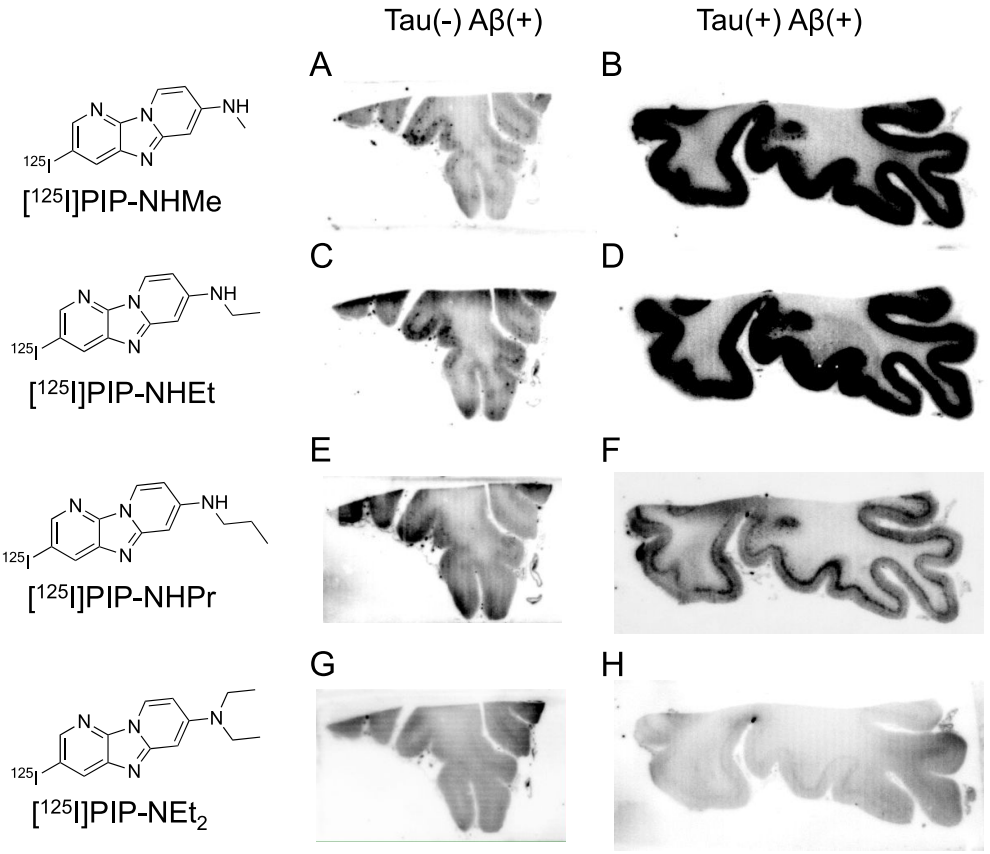

Figure 3. Comparison of in vitro autoradiography of (A, B) [^{125}I]**30** ([^{125}I]PIP-NHMe), (C, D) [^{125}I]**31** ([^{125}I]PIP-NHEt), (E, F) [^{125}I]**32** ([^{125}I]PIP-NHPr), and (G, H) [^{125}I]**40** ([^{125}I]PIP-NEt$_2$) in brain sections from an AD patient. A, C, E, and G show results in Aβ(+)/tau(−) brain sections. B, D, F, and H show results in Aβ(+)/tau(+) brain sections.

The synthetic methods used to produce BIPM and PIP derivatives are outlined in Scheme 1. The BIPM and PIP scaffolds were obtained by reaction with **3**−**8**, **33**, and **34** in the presence of 1,10-phenanthroline and cesium carbonate according to a method reported previously.[17] The tributyltin derivatives (**15**−**20**, **37**, and **38**) were obtained from the corresponding bromo compounds (**9**−**14**, **35**, and **36**) by the exchange reaction of bromine to tributyltin. The iodo compounds (**21**−**26**, **39** (BIPM-NEt$_2$), and **40** (PIP-NEt$_2$)) were obtained by the reaction of the tributyltin derivatives with I_2. Then **21**−**26** were reacted with trifluoroacetic acid (TFA) to obtain the final compounds (**27** (BIPM-NHMe), **28** (BIPM-NHEt), **29** (BIPM-NHPr), **30** (PIP-NHMe), **31** (PIP-NHEt), and **32** (PIP-NHPr)).

The radioiodinated BIPM and PIP derivatives were synthesized from the corresponding tributyltin derivatives by the iododestannylation reaction using [^{125}I]NaI and hydrogen peroxide or *N*-chlorosuccinimide (Scheme 2). As with nonradioactive compounds, [^{125}I]**27**−[^{125}I]**32** were obtained by the deprotection reaction with TFA. The radiochemical identities of these compounds were confirmed by comparison with the retention times of the corresponding nonradioactive compounds in coinjection and coelution on high-performance liquid chromatography. The radioiodinated products were obtained in radiochemical yields of 11−84% with a radiochemical purity of over 95%.

First, an in vitro autoradiographic study with two different types of AD brain sections (Aβ(+)/tau(−) and Aβ(+)/tau(+)) was carried out to evaluate the selective binding affinity to tau against Aβ aggregates according to the same method as reported in our previous studies (Figures 2 and 3).[14−17] As shown in Figure S1, Aβ aggregates were observed in the gray matter of both brain sections, whereas tau aggregates accumulated only in the gray matter of Aβ(+)/tau(+) brain sections. Accordingly, the radioactivity of ideal tau imaging probes should be specifically observed in the gray matter of Aβ(+)/tau(+) brain sections. We did not observe marked radioactivity accumulation of [^{125}I]BIPM-NHPr, [^{125}I]BIPM-NEt$_2$, and [^{125}I]PIP-NEt$_2$ in the gray matter of either Aβ(+)/tau(−) or Aβ(+)/tau(+) brain sections (Figure 2E−H and 3G,H), indicating that these compounds do not show binding affinity for either tau or Aβ aggregates. In contrast, the radioactivity of [^{125}I]PIP-NHPr slightly accumulated in the gray matter of Aβ(+)/tau(+) brain sections (Figure 3F). In addition, compared with Aβ(+)/tau(−) brain sections, [^{125}I]BIPM-NHMe, [^{125}I]BIPM-NHEt, [^{125}I]PIP-NHMe, and [^{125}I]PIP-NHEt showed higher radioactivity accumulation in the gray matter of Aβ(+)/tau(+) brain sections (Figures 2A−D and 3A−D). The accumulation pattern of [^{125}I]BIPM-NHMe, [^{125}I]BIPM-NHEt, [^{125}I]PIP-NHMe, [^{125}I]PIP-NHEt, and [^{125}I]PIP-NHPr was similar to the positive region of immunohistochemical staining with tau antibody but did not correspond with the result of immunohistochemical staining with Aβ antibody (Figure S1). The results suggested that these compounds selectively bind to tau aggregates in the AD brain sections.

Additionally, we set the regions of interest (ROIs) in the gray and white matter of both Aβ(+)/tau(−) and Aβ(+)/tau(+) brain sections and calculated the radioactivity accumulation (in

https://doi.org/10.1021/acsmedchemlett.1c00071
ACS Med. Chem. Lett. 2021, 12, 805−811

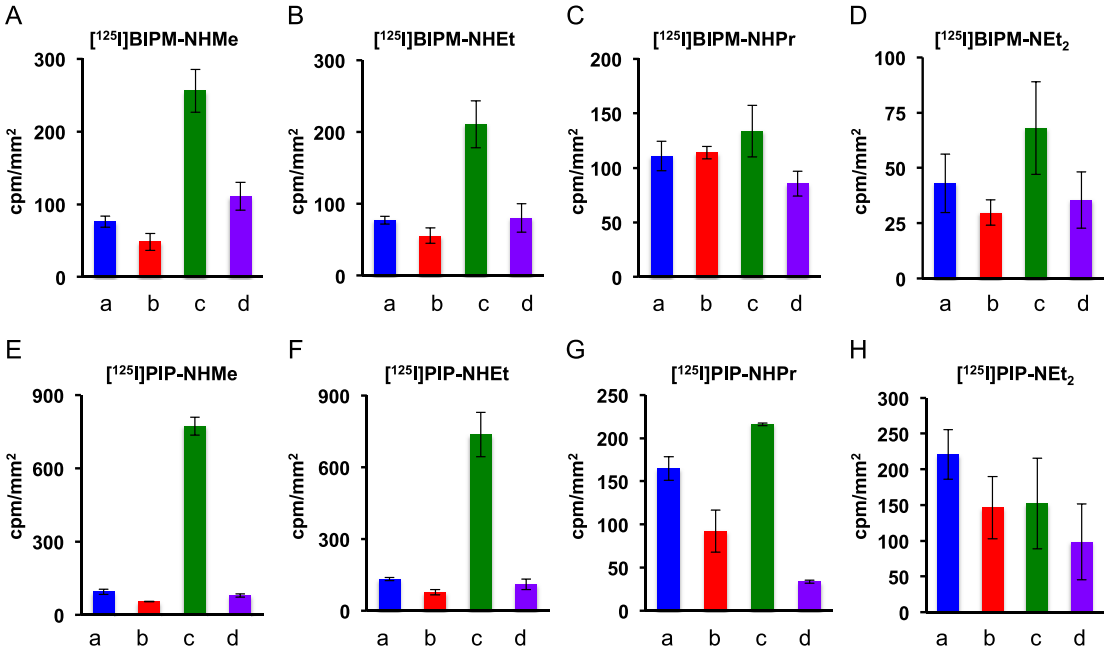

Figure 4. Quantitative analysis of [^{125}I]**27** ([^{125}I]BIPM-NHMe) (A), [^{125}I]**28** ([^{125}I]BIPM-NHEt) (B), [^{125}I]**29** ([^{125}I]BIPM-NHPr) (C), [^{125}I]**39** ([^{125}I]BIPM-NEt$_2$) (D), [^{125}I]**30** ([^{125}I]PIP-NHMe) (E), [^{125}I]**31** ([^{125}I]PIP-NHEt) (F), [^{125}I]**32** ([^{125}I]PIP-NHPr) (G), and [^{125}I]**40** ([^{125}I]PIP-NEt$_2$) (H) on *in vitro* autoradiography of AD brain sections. a: gray matter of Aβ(+)/tau(−) brain section, b: white matter of Aβ(+)/tau(−) brain section, c: gray matter of Aβ(+)/tau(+)brain section, d: white matter of Aβ(+)/tau(+) brain section.

cpm/mm^2) in each region (Figure 4). Since tau and Aβ aggregates deposited on the gray matter of brain sections, the ratio of radioactivity accumulation in the gray matter of the Aβ(+)/tau(+) brain sections against the gray matter of Aβ(+)/tau(−) brain sections was determined to quantitatively compare the selective binding affinity for tau against Aβ aggregates (Table 1). In PIP derivatives, the radioactivity in the gray matter of Aβ(+)/tau(+) brain section and the ratio for [^{125}I]PIP-NHMe (772 ± 37 cpm/mm^2 and 8.2, respectively) and [^{125}I]PIP-NHEt (736 ± 93 cpm/mm^2 and 5.6, respectively) were higher than those for [^{125}I]PIP-NHPr (216 ± 1.6 cpm/mm^2 and 1.3, respectively) and [^{125}I]PIP-NEt$_2$ (152 ± 64 cpm/mm^2 and 0.7, respectively). The same tendency was observed in BIPM derivatives, but these derivatives ([^{125}I]BIPM-NHMe and [^{125}I]BIPM-NHEt) showed lower radioactivity accumulation in the gray matter of the Aβ(+)/tau(+) brain section and a lower ratio than PIP derivatives ([^{125}I]PIP-NHMe and [^{125}I]PIP-NHEt). On the other hand, our previous study showed that radioactivity accumulation and the ratio for [^{125}I]BIPM-NMe$_2$ were higher than those for [^{125}I]PIP-NMe$_2$.[17] In addition, the ratio for [^{125}I]PIP-NHMe was higher than that of the parent dimethylamino compound ([^{125}I]PIP-NMe$_2$), but [^{125}I]BIPM-NHMe showed a lower ratio than [^{125}I]BIPM-NMe$_2$. The data for the parent compounds ([^{125}I]BIPM-NMe$_2$ and [^{125}I]PIP-NMe$_2$) were not obtained in parallel with those of the novel compounds, but these results suggest that suitable substituent groups are different between BIPM and PIP scaffolds and that optimization of the substituted group in these scaffolds may improve the selective binding affinity to tau aggregates.

Table 1. Ratio of Radioactivity Accumulation in the Gray Matter of Aβ(+)/tau(+) against Aβ(+)/tau(−) Brain Sections

compound	Aβ(+)/tau(+)/Aβ(+)/tau(−) ratio
[^{125}I]**27** ([^{125}I]BIPM-NHMe)	3.4
[^{125}I]**28** ([^{125}I]BIPM-NHEt)	2.8
[^{125}I]**29** ([^{125}I]BIPM-NHPr)	1.2
[^{125}I]**39** ([^{125}I]BIPM-NEt$_2$)	1.6
[^{125}I]BIPM-NMe$_2$[a]	6.2
[^{125}I]**30** ([^{125}I]PIP-NHMe)	8.2
[^{125}I]**31** ([^{125}I]PIP-NHEt)	5.6
[^{125}I]**32** ([^{125}I]PIP-NHPr)	1.3
[^{125}I]**40** ([^{125}I]PIP-NEt$_2$)	0.7
[^{125}I]PIP-NMe$_2$[a]	3.2

[a]The data were reported previously.[17]

Finally, we evaluated the uptake into and washout from the brain after the injection of radioiodinated BIPM and PIP derivatives by performing a biodistribution study using normal mice. As for [^{125}I]BIPM-NMe$_2$ and [^{125}I]PIP-NMe$_2$, previous data were used.[17] As shown in Table 2, all of the probes showed initial brain uptake (3.85−6.86% ID/g at 2 min postinjection) and rapid clearance (0.17−0.29% ID/g at 30 min postinjection and 0.08−0.13% ID/g at 60 min postinjection). Useful tau imaging probes should show high initial uptake into (>4% ID/g at 2 min postinjection) and rapid clearance from (<1% ID/g at 30 min postinjection) the murine brain.[18,19] [^{125}I]BIPM-NHMe and all of the PIP derivatives satisfied these criteria; especially, the brain uptakes at 2 min postinjection and the 2 min/30 min ratios for [^{125}I]PIP-NHMe (6.62% ID/g and 38.9, respectively) and [^{125}I]PIP-NHEt (6.86% ID/g and 28.6, respectively) were superior to those for [^{125}I]PIP-NMe$_2$ (5.73% ID/g and 27.3, respectively).[17] In addition, these values were higher than those for [^{125}I]BIP-NMe$_2$ (3.98% ID/g and 10.5, respectively) and [^{125}I]BIP-NHEt (6.04% ID/g and 15.5, respectively).[14,15] These results suggest that [^{125}I]PIP-NHMe and [^{125}I]PIP-NHEt have promising brain pharmacokinetics as tau imaging probes.

The same as with [^{125}I]PIP-NMe$_2$, all of the PIP derivatives showed high accumulation of radioactivity in the stomach at 60 min postinjection (13.9−18.8% ID) (Table S1). One of the

https://doi.org/10.1021/acsmedchemlett.1c00071
ACS Med. Chem. Lett. 2021, 12, 805−811

Table 2. Brain Uptakes of Radioactivity after Intravenous Injection of Radioiodinated BIPM and PIP Derivatives in Normal Mice[a] and the Ratios of Their Radioactivity Accumulations (2 min/30 min)

	% ID/g in the brain				
compd	2 min	10 min	30 min	60 min	2 min/30 min ratio
[^{125}I]**27** ([^{125}I]BIPM-NHMe)	5.50 ± 0.41	0.85 ± 0.08	0.18 ± 0.02	0.13 ± 0.03	30.5
[^{125}I]**28** ([^{125}I]BIPM-NHEt)	3.98 ± 0.18	0.83 ± 0.13	0.22 ± 0.05	0.11 ± 0.01	18.1
[^{125}I]**29** ([^{125}I]BIPM-NHPr)	3.99 ± 0.63	0.88 ± 0.04	0.22 ± 0.02	0.09 ± 0.01	18.1
[^{125}I]**39** ([^{125}I]BIPM-NEt$_2$)	3.85 ± 0.39	1.25 ± 0.20	0.29 ± 0.04	0.12 ± 0.02	13.3
[^{125}I]BIPM-NMe$_2$[b]	5.66 ± 0.34	1.00 ± 0.09	0.19 ± 0.04	0.10 ± 0.01	29.7
[^{125}I]**30** ([^{125}I]PIP-NHMe)	6.62 ± 0.84	1.73 ± 0.13	0.17 ± 0.01	0.10 ± 0.02	38.9
[^{125}I]**31** ([^{125}I]PIP-NHEt)	6.86 ± 0.96	1.97 ± 0.17	0.24 ± 0.03	0.08 ± 0.01	28.6
[^{125}I]**32** ([^{125}I]PIP-NHPr)	4.84 ± 0.39	1.10 ± 0.13	0.21 ± 0.00	0.10 ± 0.01	23.0
[^{125}I]**40** ([^{125}I]PIP-NEt$_2$)	4.54 ± 0.48	1.55 ± 0.26	0.23 ± 0.01	0.13 ± 0.01	19.7
[^{125}I]PIP-NMe$_2$[b]	5.73 ± 0.66	1.40 ± 0.32	0.21 ± 0.01	0.14 ± 0.02	27.3

[a]Each value represents the mean ± SD of five animals. [b]The data were reported previously.[17]

reasons for the radioactivity accumulation in the stomach is considered to be in vivo deiodination. However, these compounds displayed low accumulation in the thyroid (0.02−0.76% ID, respectively) at all time points, indicating that they are stable against in vivo deiodination until 60 min postinjection (Table S1). Therefore, the high accumulation in the stomach may be due to the character of the PIP scaffold.

In conclusion, we newly designed, synthesized, and evaluated radioiodinated BIPM and PIP derivatives bearing various alkylamino groups as tau imaging probes. Among the eight compounds, [^{125}I]PIP-NHMe showed the highest radioactivity accumulation in the gray matter of Aβ(+)/tau(+) brain sections and selective binding affinity for tau aggregates. In addition, favorable pharmacokinetics in the murine brain was observed. These results suggest that [^{123}I]PIP-NHMe has potential as a novel tau imaging probe for SPECT.

■ ASSOCIATED CONTENT

Supporting Information

The Supporting Information is available free of charge at https://pubs.acs.org/doi/10.1021/acsmedchemlett.1c00071.

Full experimental methods, results of immunohistochemical staining, and biodistribution study for all organs (PDF)

■ AUTHOR INFORMATION

Corresponding Authors

Hiroyuki Watanabe − *Department of Patho-Functional Bioanalysis, Graduate School of Pharmaceutical Sciences, Kyoto University, Kyoto 606-8501, Japan*; orcid.org/0000-0002-8873-1224; Phone: +81-75-753-4607; Email: hwatanabe@pharm.kyoto-u.ac.jp; Fax: +81-75-753-4568

Masahiro Ono − *Department of Patho-Functional Bioanalysis, Graduate School of Pharmaceutical Sciences, Kyoto University, Kyoto 606-8501, Japan*; orcid.org/0000-0002-2497-039X; Phone: +81-75-753-4556; Email: ono@pharm.kyoto-u.ac.jp; Fax: +81-75-753-4568

Authors

Takeaki Kishimoto − *Department of Patho-Functional Bioanalysis, Graduate School of Pharmaceutical Sciences, Kyoto University, Kyoto 606-8501, Japan*

Sho Kaide − *Department of Patho-Functional Bioanalysis, Graduate School of Pharmaceutical Sciences, Kyoto University, Kyoto 606-8501, Japan*

Yuta Tarumizu − *Department of Patho-Functional Bioanalysis, Graduate School of Pharmaceutical Sciences, Kyoto University, Kyoto 606-8501, Japan*

Haruka Tatsumi − *Department of Patho-Functional Bioanalysis, Graduate School of Pharmaceutical Sciences, Kyoto University, Kyoto 606-8501, Japan*

Shimpei Iikuni − *Department of Patho-Functional Bioanalysis, Graduate School of Pharmaceutical Sciences, Kyoto University, Kyoto 606-8501, Japan*; orcid.org/0000-0002-7073-9084

Complete contact information is available at: https://pubs.acs.org/10.1021/acsmedchemlett.1c00071

Notes

The authors declare no competing financial interest.

■ ACKNOWLEDGMENTS

This research was supported by JSPS KAKENHI Grants JP17H05092 and JP17H05694. We thank Dr. Masafumi Ihara (National Cerebral and Cardiovascular Center) for providing brain samples of AD cases.

■ REFERENCES

(1) Prince, M.; Wimo, A.; Guerchet, M.; Ali, G.-C.; Wu, Y.-T.; Prina, M., *World Alzheimer Report 2015: The Global Impact of Dementia: An Analysis of Prevalence, Incidence, Cost and Trends*; Alzheimer's Disease International: London, 2015.

(2) Gavrilova, S. I.; Alvarez, A. Cerebrolysin in the therapy of mild cognitive impairment and dementia due to Alzheimer's disease: 30 years of clinical use. *Med. Res. Rev.* **2020**, DOI: 10.1002/med.21722.

(3) Villemagne, V. L.; Fodero-Tavoletti, M. T.; Masters, C. L.; Rowe, C. C. Tau imaging: early progress and future directions. *Lancet Neurol.* **2015**, *14* (1), 114−124.

(4) Harada, R.; Okamura, N.; Furumoto, S.; Yanai, K. Imaging Protein Misfolding in the Brain Using β-Sheet Ligands. *Front. Neurosci.* **2018**, *12*, 585.

(5) Villemagne, V. L.; Dore, V.; Burnham, S. C.; Masters, C. L.; Rowe, C. C. Imaging tau and amyloid-β proteinopathies in Alzheimer disease and other conditions. *Nat. Rev. Neurol.* **2018**, *14* (4), 225−236.

(6) Leuzy, A.; Chiotis, K.; Lemoine, L.; Gillberg, P. G.; Almkvist, O.; Rodriguez-Vieitez, E.; Nordberg, A. Tau PET imaging in neurodegenerative tauopathies-still a challenge. *Mol. Psychiatry* **2019**, *24* (8), 1112−1134.

(7) Beyer, L.; Brendel, M. Imaging of Tau Pathology in Neurodegenerative Diseases: An Update. *Semin. Nucl. Med.* **2021**, *51* (3), 253−263.
(8) Fleisher, A. S.; Pontecorvo, M. J.; Devous, M. D., Sr.; Lu, M.; Arora, A. K.; Truocchio, S. P.; Aldea, P.; Flitter, M.; Locascio, T.; Devine, M.; Siderowf, A.; Beach, T. G.; Montine, T. J.; Serrano, G. E.; Curtis, C.; Perrin, A.; Salloway, S.; Daniel, M.; Wellman, C.; Joshi, A. D.; Irwin, D. J.; Lowe, V. J.; Seeley, W. W.; Ikonomovic, M. D.; Masdeu, J. C.; Kennedy, I.; Harris, T.; Navitsky, M.; Southekal, S.; Mintun, M. A. Positron Emission Tomography Imaging With [^{18}F]flortaucipir and Postmortem Assessment of Alzheimer Disease Neuropathologic Changes. *JAMA Neurol.* **2020**, *77* (7), 829−839.
(9) Betthauser, T. J.; Cody, K. A.; Zammit, M. D.; Murali, D.; Converse, A. K.; Barnhart, T. E.; Stone, C. K.; Rowley, H. A.; Johnson, S. C.; Christian, B. T. In Vivo Characterization and Quantification of Neurofibrillary Tau PET Radioligand ^{18}F-MK-6240 in Humans from Alzheimer Disease Dementia to Young Controls. *J. Nucl. Med.* **2019**, *60* (1), 93−99.
(10) Kuwabara, H.; Comley, R. A.; Borroni, E.; Honer, M.; Kitmiller, K.; Roberts, J.; Gapasin, L.; Mathur, A.; Klein, G.; Wong, D. F. Evaluation of F-18-RO-948 PET for Quantitative Assessment of Tau Accumulation in the Human Brain. *J. Nucl. Med.* **2018**, *59* (12), 1877−1884.
(11) Mueller, A.; Bullich, S.; Barret, O.; Madonia, J.; Berndt, M.; Papin, C.; Perrotin, A.; Koglin, N.; Kroth, H.; Pfeifer, A.; Tamagnan, G. D.; Seibyl, J. P.; Marek, K.; De Santi, S.; Dinkelborg, L. M.; Stephens, A. W. Tau PET imaging with F-18-PI-2620 in Patients with Alzheimer Disease and Healthy Controls: A First-in-Humans Study. *J. Nucl. Med.* **2020**, *61* (6), 911−919.
(12) Sanabria Bohorquez, S.; Marik, J.; Ogasawara, A.; Tinianow, J. N.; Gill, H. S.; Barret, O.; Tamagnan, G.; Alagille, D.; Ayalon, G.; Manser, P.; Bengtsson, T.; Ward, M.; Williams, S. P.; Kerchner, G. A.; Seibyl, J. P.; Marek, K.; Weimer, R. M. [^{18}F]GTP1 (Genentech Tau Probe 1), a radioligand for detecting neurofibrillary tangle tau pathology in Alzheimer's disease. *Eur. J. Nucl. Med. Mol. Imaging* **2019**, *46* (10), 2077−2089.
(13) Tagai, K.; Ono, M.; Kubota, M.; Kitamura, S.; Takahata, K.; Seki, C.; Takado, Y.; Shinotoh, H.; Sano, Y.; Yamamoto, Y.; Matsuoka, K.; Takuwa, H.; Shimojo, M.; Takahashi, M.; Kawamura, K.; Kikuchi, T.; Okada, M.; Akiyama, H.; Suzuki, H.; Onaya, M.; Takeda, T.; Arai, K.; Arai, N.; Araki, N.; Saito, Y.; Trojanowski, J. Q.; Lee, V. M. Y.; Mishra, S. K.; Yamaguchi, Y.; Kimura, Y.; Ichise, M.; Tomita, Y.; Zhang, M. R.; Suhara, T.; Shigeta, M.; Sahara, N.; Higuchi, M.; Shimada, H. High-Contrast In Vivo Imaging of Tau Pathologies in Alzheimer's and Non-Alzheimer's Disease Tauopathies. *Neuron* **2021**, *109* (1), 42−58.
(14) Ono, M.; Watanabe, H.; Kitada, A.; Matsumura, K.; Ihara, M.; Saji, H. Highly Selective Tau-SPECT Imaging Probes for Detection of Neurofibrillary Tangles in Alzheimer's Disease. *Sci. Rep.* **2016**, *6*, 34197.
(15) Kaide, S.; Ono, M.; Watanabe, H.; Kitada, A.; Yoshimura, M.; Shimizu, Y.; Ihara, M.; Saji, H. Structure-Activity Relationships of Radioiodinated Benzoimidazopyridine Derivatives for Detection of Tau Pathology. *ACS Med. Chem. Lett.* **2018**, *9* (5), 478−483.
(16) Kaide, S.; Watanabe, H.; Shimizu, Y.; Tatsumi, H.; Iikuni, S.; Nakamoto, Y.; Togashi, K.; Ihara, M.; Saji, H.; Ono, M. ^{18}F-labeled benzimidazopyridine derivatives for PET imaging of tau pathology in Alzheimer's disease. *Bioorg. Med. Chem.* **2019**, *27* (16), 3587−3594.
(17) Watanabe, H.; Tatsumi, H.; Kaide, S.; Shimizu, Y.; Iikuni, S.; Ono, M. Structure-Activity Relationships of Radioiodinated 6,5,6-Tricyclic Compounds for the Development of Tau Imaging Probes. *ACS Med. Chem. Lett.* **2020**, *11* (2), 120−126.
(18) Mason, N. S.; Mathis, C. A.; Klunk, W. E. Positron emission tomography radioligands for in vivo imaging of Aβ plaques. *J. Labelled Compd. Radiopharm.* **2013**, *56* (3−4), 89−95.
(19) Okamura, N.; Harada, R.; Furumoto, S.; Arai, H.; Yanai, K.; Kudo, Y. Tau PET imaging in Alzheimer's disease. *Curr. Neurol. Neurosci. Rep.* **2014**, *14* (11), 500.

https://doi.org/10.1021/acsmedchemlett.1c00071
ACS Med. Chem. Lett. 2021, 12, 805−811